EPR, ENDOR, and optical spectroscopy of the tetragonal Yb^{3+} center in $KMgF_3$

M. L. Falin and V. A. Latypov
Zavoisky Physical-Technical Institute, Kazan, Russian Federation

B. N. Kazakov and A. M. Leushin
Kazan State University, Kazan, Russian Federation

H. Bill and D. Lovy
Group CPB, University of Geneva, Geneva, Switzerland

(Received 20 July 1999; revised manuscript received 29 October 1999)

Electron paramagnetic resonance, electron-nuclear double resonance, and optical spectroscopy of the tetragonal Yb^{3+} center in $KMgF_3$ are reported here. The results of these experiments allow us to conclude that a previously given structural model as well as the interpretation of the optical spectrum of this center are incorrect. A model is presented and experimentally and theoretically justified. In particular, the values of the hyperfine and transferred hyperfine interaction parameters were determined as well as an experiment-based energy-level scheme. Its parametrization is performed by including simultaneously the crystal field and the spin-orbit interaction within the ^7F term. Furthermore, a theoretical analysis of the transferred hyperfine interaction (THFl) parameters is presented. It is further shown from optics and from microscopic calculations of the THFI parameters that $g_\parallel$ and $g_\perp$ have opposite signs and that the rule of correspondence between the cubic g factor and $\tilde{g}=\frac{1}{3}(g_x+g_y+g_z)$ does not depend on the relative magnitude of the cubic and low-symmetry crystal field acting on the rare-earth ion.

INTRODUCTION

Ternary fluoride crystals with the perovskite structure ABF_3 (A^+,B^{2+}) are very interesting because on the one hand they find extensive practical applications and on the other hand they are convenient model hosts for transition metal (TM) or rare-earth (RE) impurity ions when the magneto-optical properties of these ions are investigated. These crystals possess two different host cation sites: B^{2+} is six coordinated whereas A^+ has coordination number 12 (which is rather uncommon). In principle impurity cations can be introduced on both sites. This dissimilarity in coordination leads to essentially differing crystal fields and thus often to importantly modified magnetic and optical properties of the suitably chosen impurities. Note that even the mere definition of the structural model, i.e., the detailed location of the impurity ion and its exact surrounding is in general not a simple problem. To a certain degree the RE impurities are exceptions as the shielding of the unfilled $4f$-shell electrons by the closed $5s$ and $5p$ shells considerably reduces the effects of the crystal field (CF). Its interaction energy is significantly less than the one of the spin-orbit interaction with the result that the crystal field does not scramble the scheme of the free ion energy spectrum. When considered as a perturbation it will in first order lower or remove the $(2J+1)$-fold degeneracy of the multiplets and slightly mix (in second-order perturbation theory) states with different J. Basic patterns of the splitting of the RE ion multiplets in a cubic crystal field are given by group theory and, for levels transforming according to different irreducible representations (IREP), the basis states are completely defined by symmetry. If more than one level transforms according to the same IREP then their respective wave functions depend on the ratio of the B_4^0 and B_6^0 crystal-field parameters.[1] Knowledge of the wave functions unambiguously determines the g factors. This in turn enables to obtain (or to verify) the coordination of the nearest surrounding of the ion within the framework of the point-charge model. When a distortion of the crystal lowers the CF from cubic to lower symmetry and if this perturbation is small in comparison with the cubic contribution, then for RE ions with an odd number of f electrons the rule of the average g factor $\tilde{g}=\frac{1}{3}(g_x+g_y+g_z)\cong g_{\mathrm{cub}}$ applies.[2] Using this relation to obtain $\tilde{g}$ from the experimental results in conjunction with analytical solutions for the isotropic g factor of the cubic Γ_6 and Γ_7 Kramers doublets obtained on the basis of the point-charge model allows us to reach conclusions about the coordination of the RE ion and to predict the structural model of the paramagnetic center (PC). This rule provides a basis for a coherent analysis of the coordination of a RE ion from electron paramagnetic resonance (EPR) experiments. The EPR study of Yb^{3+} in $KMgF_3$ (Ref. 3) is a typical example of this approach. Comparison between the experimentally determined value of $\tilde{g}$ with theoretical predictions obtained as described above allowed us to conclude that the observed cubic and trigonal PC's correspond to Yb^{3+} ions on octahedral sites (i.e., substituting a Mg^{2+} ion), whereas the tetragonal Yb^{3+} PC was found to be located on a 12-fold coordinated K^+ host cation site. Detailed structures of the PC's were further proposed in the paper by Abraham *et al.*[3] The symmetry lowering was attributed to the formation of K^+ ion vacancies adjacent to the RE ion: one vacancy on a trigonal axis would produce the trigonal PC whereas two vacancies in adjacent positions on one common tetragonal axis would give the tetragonal PC. A subsequent electron-nuclear double resonance investigation (ENDOR) (Refs. 4–6) allowed us to confirm the mod-

els of the cubic and the trigonal PC.

But the model of the tetragonal PC led to an inconsistent interpretation of the optical spectra of Yb^{3+} in $KMgF_3$.[7] In particular, the conclusion had been reached that the CF operating on the RE ion at the K^+ site was extremely small. Further, the results published in Refs. 3 and 7 yielded several contradictory conclusions which did not agree with the given model. They were:

(i) the experimental g factor is highly *anisotropic*, in contradiction to the results of the weak crystal-field model;

(ii) the EPR spectra show a doublet structure on the high-field lines ($H \| z$) and a superhyperfine structure (SHFS) on the low-field ones ($H \perp z$). The model[3,7] cannot account for the former structure and the latter one can be explained by other models;

(iii) a significant difference is observed between the splitting of the $^2F_{5/2}$ multiplet for the cubic and trigonal Yb^{3+}PC($\sim 1000\,cm^{-1}$) on one side and the tetragonal PO ($\sim 75\ cm^{-1}$) on the other side.

A recent experimental ENDOR investigation[8] presented preliminary results of the tetragonal Yb^{3+} center in $KMgF_3$ crystals which showed that in this case the Yb^{3+} substitutes for a Mg^{2+} ion and not for a K^+ one. For this situation the question of whether the average g factor rule can be applied needed to be reinvestigated.

Our previous optical investigation of cubic Yb^{3+} ions in $CsCaF_3$ (Ref. 9) (12-coordinated) showed that the CF of this center is not weak. It is even comparable with the CF of rare-earth fluorides.

The present paper gives the results of a detailed investigation of the tetragonal Yb^{3+} PC in the single-crystal host $KMgF_3$ by EPR, ENDOR, and optical spectroscopy. These results unambiguously demonstrate that contrary to the proposed model[3,7] the tetragonal PC has an octahedral surrounding. The compensation of the excess positive charge is realized by a nonmagnetic oxygen ion which substitutes for one of the fluorine ions in the nearest-neighbor octahedron. The resulting tetragonal crystal field is very high and is comparable to the one observed for cubic and trigonal Yb^{3+}PC's in this same host matrix. Then, we show that $g_\parallel$ and $g_\perp$ have opposite signs. We further extend the above-mentioned rule of the correspondence between g defined above and the cubic g factor.

EXPERIMENT

$KMgF_3$:Yb^{3+} single crystals were grown by the Czochralski method under a helium atmosphere. Ytterbium was inserted into the melt as YbF_3 or Yb_2O_3. EPR and ENDOR spectra were recorded at $T = 4.2$ K on a homebuilt EPR and ENDOR spectrometer based on an E 110 Varian *X*-band equipment and on an EPR-231 spectrometer modified by adjoining an ENDOR attachment. The EPR spectrum of omnipresent Mn^{2+} was observed in all samples.

Optical spectra were recorded on a computerized spectrometer (600 lines/mm grating, 4 nm/mm inverse linear dispersion). A cooled photomultiplier formed the detector and the light of a xenon lamp dispersed by a prism monochromator was used as an excitation source. As the transitions are almost merely electronic (resonance excitation) the luminescence and excitation spectra were recorded by using time delayed (stroboscopic) detection. The spectral lines of the different PC's were further discriminated by using the modified phase-modulation method.[10,11] The essence of modification consisted in the following.[12] The excitation light beam was modulated by a symmetrical square wave. The luminescence signal observed at the output of the photomultiplier was subjected to a linear integral transformation which consisted in the multiplication of the signal by a Walsh function and its integration over the modulation period. Note that the usual procedure consists in multiplication by a harmonic function and subsequent integration over the modulation period. By varying systematically the time shift x of the Walsh function one obtains a value $x = x_0$ where the result of transformation is equal to zero. By entering this value into an appropriate transcendental equation one obtains numerical values of the lifetime of the luminescence. This transformation was realized as a hardware setup with the aid of a sequential filter based on switched capacitors.[13] The Walsh function determines the shape of the reference signal and the parameter x—its time shift.

EXPERIMENTAL RESULTS

EPR, ENDOR

The angular dependence of the EPR spectrum of the tetragonal Yb^{3+} center is shown in Fig. 1. It was recorded with **H** being rotated in a (001) plane. Note further the presence of some lines of the cubic and the trigonal centers. The high-field EPR lines formed a resolved doublet structure between $\vartheta = 0°$ ($\mathbf{H} \| z$) and $\vartheta = 10°$ whereas the low-field lines, observed for $\mathbf{H} \perp z$, presented partly resolved SHFS. In the situations where ENDOR was observed on the lines the magnetic-field angle could be aligned to better than 0.05°. The inserts of the figure present the details of the low-field ($\mathbf{H} \perp z$) and high-field ($\mathbf{H} \| z$) EPR spectra of the isotopes $^{171,173}Yb^{3+}$. The hyperfine structure of the high-field EPR lines clearly shows significant second-order effects. The absence of SHFS on the low-field EPR lines (see inset Fig. 1) is due to modulation broadening as the weak signals obliged us to work with a high magnetic-field modulation amplitude. The EPR parameters of this center together with those obtained by Abraham *et al.*[3] on this PC and the analogous results for the cubic one are given in Table I. The dashed lines in Fig. 1 present the angular dependence of the EPR spectrum calculated with our parameters.

Another type of cubic Yb^{3+} spectrum further was found (labeled ''cub′'' in Fig. 1). We assumed that this center consisted of an Yb^{3+} ion substituting for a K^+ ion because this PC had properties similar to those observed by us on a Yb^{3+} PC in $CsCaF_3$.[14]

Most of the ENDOR experiments were carried out on the even Yb^{3+} isotope. Nearly all the spectra were obtained on the high-field EPR lines, despite the weak intensity of the latter. Figure 2 shows representative ENDOR spectra. A detailed analysis of the spectra and their angular dependence (Fig. 3) yielded that the Yb^{3+} ion substitutes for a Mg^{2+} ion and that the local compensation of the excess positive charge is provided by a nonmagnetic impurity anion which replaces

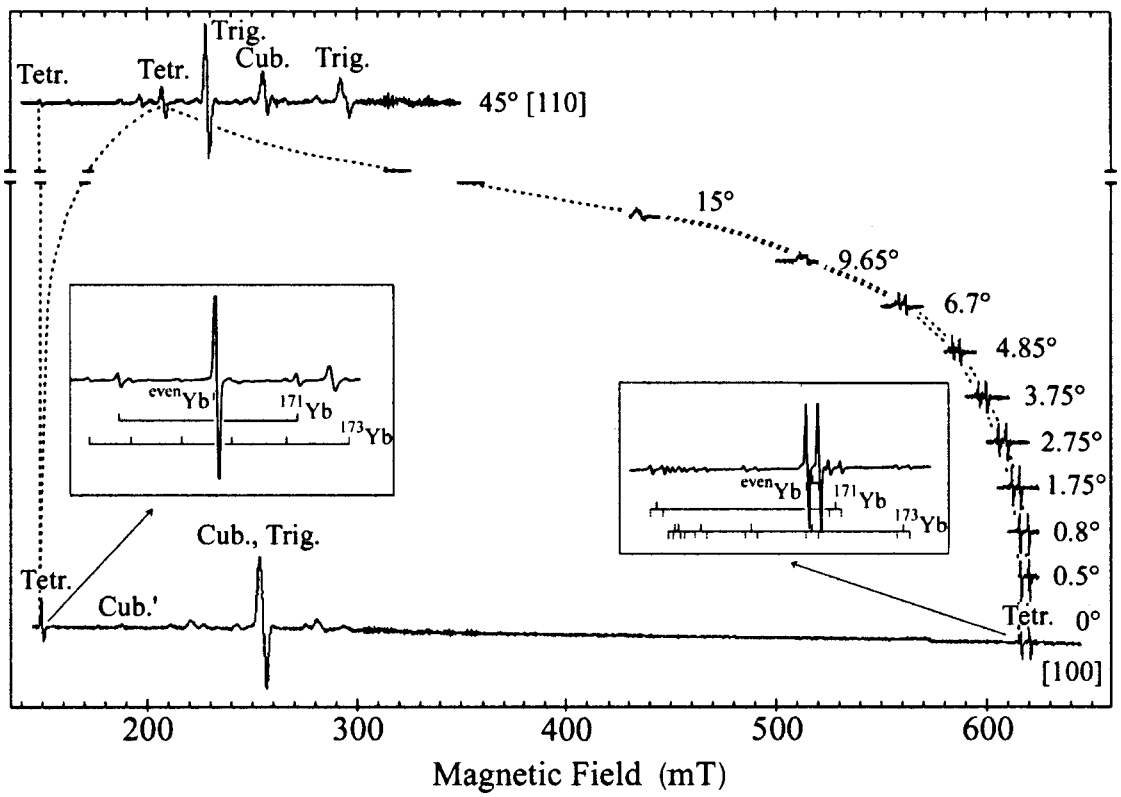

FIG. 1. EPR spectra of Yb^{3+} in $KMgF_3$, with **H** in a (001) plane. $T=4.2$ K, $\nu=9.265$ GHz. Insets show the hyperfine structure of the EPR spectra of Yb^{3+} in $KMgF_3$ for **H** parallel and perpendicular to the tetragonal axis of the complex. The dashed lines indicate the experimental splitting of the hyperfine transitions. The theoretical curves of the angular dependence of the EPR lines (dashed lines) of the tetragonal Yb^{3+} ion were obtained by using the data of Table I (see text).

one of the six fluorine neighbors. The Discussion section presents arguments showing that the PC consists of a $[YbOF_5]^{4-}$ unit (Fig. 4—where its principal axes are defined). This PC has local C_{4v} symmetry and thus no inversion center. The local symmetry of the ions $F_1^-(i=1,...,4)$ is C_s and is C_{4v} for F_5^- and the oxygen ion. Thus the transferred hyperfine interaction (THFI) tensors have five and two independent components, respectively. The ENDOR spectra were described by the standard THFI spin Hamiltonian

$$H=\beta HgS+\sum_i (SA^{(i)}I_F^{(i)}-\beta_n Hg_n'^{(i)}I_F^{(i)}), \qquad (1)$$

where $S=I_F^{(i)}=\frac{1}{2}$, the quantities $A^{(i)}$ are the THFI tensors, i labels the nuclei, $g_n^F=5.254\,54$.

The one-particle nuclear Hamiltonian (1) was averaged over the electron variables up to second-order perturbation theory and then diagonalized. General expressions for the ENDOR transition frequencies were obtained for arbitrary orientations of the magnetic field **H** with respect to the crystallographic axes by using the selection rules for ENDOR transitions (see also Ref. 15).

$$\nu_i=[a_i^2C_i^2+(b_iC_2+C_5)^2+(C_3+b_iC_4)^2]^{1/2}, \qquad (2)$$

where $i=F_1^-,F_2^-,F_3^-,F_4^-$,

TABLE I. EPR parameters of Yb^{3+} in $KMgF_3$. The values of the hyperfine interaction parameters A are in $10^{-4}\,cm^{-1}$, $\tilde{g}=\frac{1}{3}(g_\parallel+2g_\perp)$. The negative sign of the g factor for cubic Yb^{3+} was determined theoretically (Ref. 1).

$g_\parallel$	$g_\perp$	$\tilde{g}$	Ground state	$^{171}A_\parallel$	$^{171}A_\perp$	$^{173}A_\parallel$	$^{173}A_\perp$	
|1.070 (1)|	|4.430(3)|	3.31	Γ_7	|281.0(5)|	|1166(2)|	|74(1)|	|344(2)|	a
1.070	−4.430	−2.597	Γ_6					b
|1.078|	|4.377|	3.277	Γ_7					c
	(−)2.584		Γ_6	684.7		188.5		c

[a]This work. Experiment.

[b]This work. From optics and microscopic calculation of the THFI parameters (see text).

[c]Reference 3.

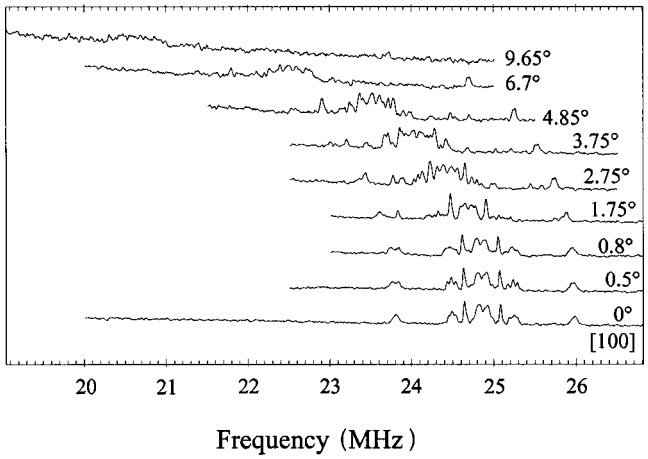

FIG. 2. ENDOR spectra of Yb^{3+} in $KMgF_3$. The magnetic field was rotated in the (001) plane, $T=4.2$ K, $\nu=9.265$ GHz.

$$C_1=\left\{\frac{g_\perp}{g}[MA_1-\mu_-(M)(A_2A_3-A_4A_5)]-\beta_n g_n^F H\right\}\sin\vartheta,$$

$$C_2=\left\{\frac{g_\perp}{g}[MA_2-\mu_-(M)A_1A_3]\right\}\sin\vartheta,$$

$$C_3=\left\{\frac{g_\parallel}{g}[MA_3-\mu_-(M)A_1A2]-\beta_n g_n^F H\right\}\cos\vartheta,$$

$$C_4=\left\{\frac{g_\perp}{g}[MA_4-\mu_-(M)A_1A_5]\right\}\sin\vartheta,$$

$$C_5=\left\{\frac{g_\parallel}{g}[MA_5-\mu_-(M)A_1A4]\right\}\cos\vartheta,$$

$$a_{1,3}=\cos\varphi,\quad a_{2,4}=\sin\varphi,$$

$$b_{1,3}=\pm\sin\varphi,\quad b_{2,4}=\pm\cos\varphi,$$

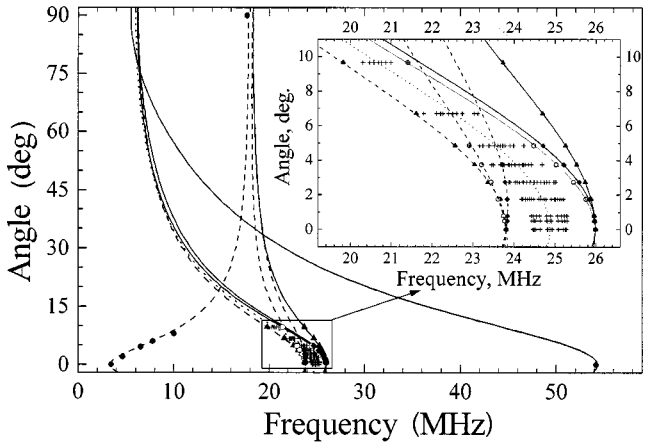

FIG. 3. Angular dependence of the ENDOR lines of the first fluorine shell with **H** in an (001) plane. Experimental data points: ●↔F_5^-; ▲↔$F_{1,3}^-$; ◆, ○↔$F_{2,4}^-$, +↔ distant fluorine. The theoretical curves were obtained by using the data of Table II (solid and dashed lines for $M=\pm\frac{1}{2}$, respectively). The dotted line represents the fluorine Larmor frequency as a function of the orientation of the magnetic field.

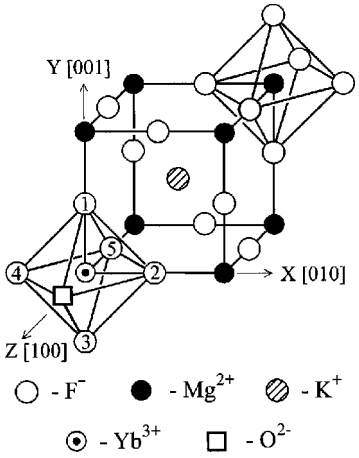

FIG. 4. Fragment of the structure of $KMgF_3$.

$$\mu_-(M)=\frac{S(S+1)-M^2}{2g\beta H},$$

$$g=(g_\parallel^2\cos^2\vartheta+g_\perp^2\sin^2\vartheta)^{1/2}.$$

The plus and minus signs in $a_{i,j}, b_{i,j}$ refer to $F_{1,3}^-$ and $F_{2,4}^-$ respectively; ϑ, φ are the polar angles; M is the magnetic quantum number of the electron spin. The THFI tensor of F_5^- is characterized by $A_1=A_2$ and $A_4=A_5=0$. Then, the expressions for the ENDOR transition frequencies simplify to

$$\nu(F_5^-)=(C_1^2\cos^2\vartheta+C_3^2\sin^2\vartheta)^{1/2}. \tag{3}$$

Since the ENDOR spectra were investigated with **H** parallel to (001) the expressions Eqs. (2) were simplified by adopting $\varphi=0°$.

The experimental THFI parameters were obtained by the least-squares method with the aid of Eqs. (2) and (3). The obtained parameters are given in Table II together with the results for the cubic Yb^{3+} in $KMgF_3$,[4] for convenient comparison. The signs of the THFI parameters were determined according to Zaripov, Meiklyar, and Falin[16] by taking into account the fact that the signs of $g_\parallel$ and $g_\perp$ are mutually opposite (see Discussion section).

Additional confirmation of the correctness of the THFI parameter determination and of the model of the complex was obtained by the numerical simulation of the line shape

TABLE II. The experimental values of the THFI parameters A_i (in MHz) and B_s (in 10^{-4} T) of the first fluorine shell of Yb^{3+} in $KMgF_3$. The results for the cubic center of Yb^{3+} in $KMgF_3$ are given for comparison.

	F_{1-4}^-	F_5^-	Cubic[a]
A_1	−24.60(3)	57.63(5)	29.211
A_2	24.46(3)	57.63(5)	29.211
A_3	2.18(3)	23.3(1)	11.416
A_4	0.0(1)		
A_5	2.84(3)		
B_s	−3.24	−15.4	(−)6.42

[a]Reference 4.

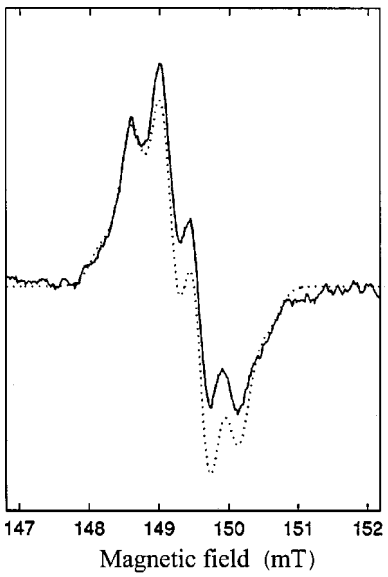

FIG. 5. Experimental and simulated (dashed line) EPR spectra of Yb^{3+} in $KMgF_3$ for $\mathbf{H}\perp z$, $T=4.2$ K, $\nu=9.265$ GHz.

of the low-field EPR line for $\mathbf{H}\perp z$. Figure 5 demonstrates the good agreement reached between the calculated and the observed spectrum.

Optical spectroscopy

The near-infrared luminescence spectrum obtained from a $KMgF_3$:Yb^{3+} crystal is shown in Fig. 6(a) (recorded at room temperature) and Fig. 6(b) (at 77 K). The transitions which correspond to the tetragonal Yb^{3+} PC are labeled by arrows. The optical-absorption spectrum of the *f-f* transitions was not observed, due to the low concentration of Yb^{3+} ions in our crystals. But the excitation spectrum of Yb^3 allowed to obtain them [Fig. 6(c)].

The analysis of the spectra showed that the emission lines labeled 1,2,3,4 in Figs. 6(a) and 6(b) were due to transitions from the lower Stark level of the exited multiplet $^2F_{5/2}$ of the Yb^{3+} to the four Stark components of the ground multiplet $^2F_{7/2}$. The spectral components labeled 4, 5, and 6 in the excitation spectrum [Fig. 6(c)] corresponded to transitions from the lower levels of $^2F_{7/2}$ to the three Stark components of $^2F_{5/2}$. Comparison of the luminescence and the excitation spectra yielded that line 4 was an electronic transition between the same energy levels in emission as well as in absorption. The indexing of the spectral lines given in Figs. 6(a)–(c) corresponds to the labeling of the transitions on the experimental energy level diagram of Yb^{3+} (Fig. 7).

In order to interpret the transitions within the ^2F term (configuration $4f^{13}$) we constructed an energy matrix which included the spin-orbit interaction of the Yb^{3+} ion, the crystal field and the Zeeman interaction with an external magnetic field. The form of the tetragonal crystal-field potential written in standard notation is

$$H_{\mathrm{cr}}(C_{4\nu})=B_2^0V_2^0+B_4^0V_4^0+B_4^4V_4^4+B_6^0V_6^0+B_6^4V_6^4.$$

The V_k^q are standard harmonic polynomials.[17] The Cartesian coordinate frame shown in Fig. 4 was used for the $4f$ hole wave function. The crystal-field parameters and the spin-orbit interaction ξ were obtained according to the procedure described by Bespalov *et al.*[18] Thereby the best fit of the level scheme and the g values was obtained in a least-square sense. During this fitting process it became clear that the model of the tetragonal PC is only possible if the crystal field acting on the Yb^{3+} is very strong, and that the measured g factors have opposite signs. The theoretical values of the energy levels, the g factors and the symmetry labeled wave functions obtained according to this procedure are given in Table III. The standard deviation did not exceed 5 cm^{-1}. The theoretical values of the crystal-field parameters and of the spin-orbit interaction constant are given in Table IV together with the corresponding quantities of the cubic and the trigonal Yb^{3+} PC's.[19]

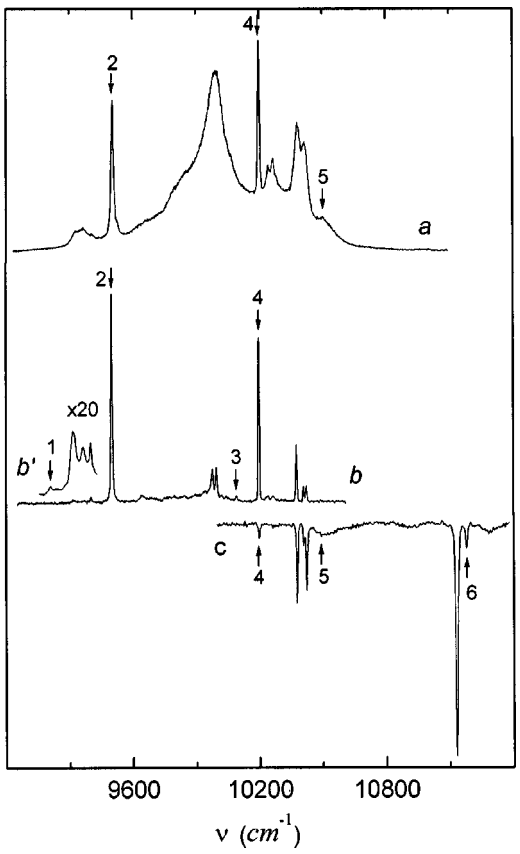

FIG. 6. Luminescence spectra of Yb^{3+} in $KMgF_3$ at $T=300$ K (a), $T=77$ K (b) and $T=4.2$ K (b′); excitation spectrum at $T=77$ K (c). Optical transitions corresponding to the tetragonal PC center are marked by arrows. Numbering of the spectral lines corresponds to the numbering of the transitions in Fig. 7.

DISCUSSION

The tetragonal Yb^{3+} PC was only observed in crystals which had been doped by Yb_2O_3. This fact and the following arguments show that most probably an O^{2-} ion substitutes for one of the fluorine ions in the nearest-neighbor coordination shell. As shown in Table IV the crystal-field potential of the tetragonal PC corresponds to a highly distorted cubic structure, in opposition to the trigonal PC. This distortion is conditioned by the very powerful tetragonal CF created by the excess negative charge of the nearest-neighbor oxygen ion compensating the charge of the Yb^{3+}. The large splitting

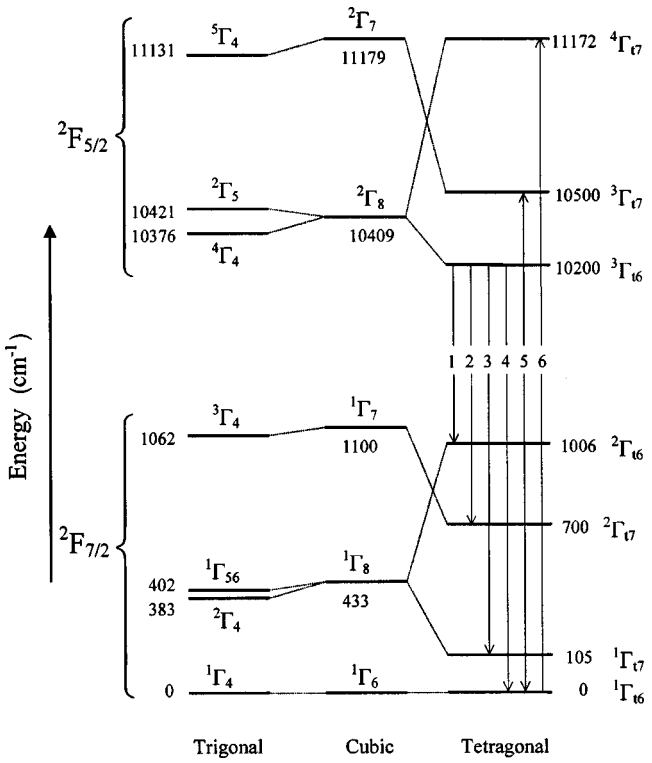

FIG. 7. Experimental energy-level diagrams for the ground ($^2F_{7/2}$) and the excited ($^2F_{5/2}$) multiplets for Yb^{3+} of cubic (Ref. 19), trigonal (Ref. 19), and tetragonal symmetry in $KMgF_3$ (in cm^{-1}). The transitions observed in the optical spectra (Fig. 6) are represented by the arrows.

of the cubic quartet and the energy shift of the doublet levels due to the tetragonal CF demonstrate the important deviation from cubic symmetry of the latter for the tetragonal PC. This can be assessed by inspecting the energy-level diagram Fig. 7. This figure further shows that contrary to Antipin *et al.*[7] a CF of comparable strength with respect to the one of the cubic and trigonal Yb^{3+}PC is obtained for the tetragonal RE ion center.

Very strong mixing of the cubic wave functions is observed in the basis functions of the Kramers doublets of the tetragonal PC. For instance, the wave functions of the lower Kramers doublet $^1\Gamma_{t6}$ display the following structure:

$$\left|{}^1\Gamma_{t6}\pm\frac{1}{2}\right\rangle = \pm 0.991\,06\left|\frac{7}{2},\pm\frac{1}{2}\right\rangle \pm 0.133\,28\left|\frac{7}{2};\mp\frac{7}{2}\right\rangle + 0.005\,51\left|\frac{5}{2};\pm\frac{1}{2}\right\rangle,$$

where in the states $|J;M_J\rangle J$ labels the total angular momentum of the given multiplet, and M_J is its projection on the Z axis of the PC. The fact that the ratios ($|g_\perp A_\parallel / g_\parallel A_\perp|$) are close to one (0.998 for $^{171}Yb^{3+}$ and 0.891 for $^{173}Yb^{3+}$, see Table I) also confirms that the influence of the other, higher lying, J states can be neglected. If the two functions are constructed as linear combinations of cubic states[20] we obtain

$$\left|{}^1\Gamma_{t6}\pm\frac{1}{2}\right\rangle = -0.842\,97\left|{}^1\Gamma_6^-\pm\frac{1}{2}\right\rangle - 0.537\,93\left|{}^1\Gamma_8^-\pm\frac{1}{2}\right\rangle + 0.005\,51\left|{}^2\Gamma_8^-\pm\frac{1}{2}\right\rangle.$$

In this representation it becomes evident that the contribution of the cubic doublet Γ_6^- is dominant. As this one is the lowest level for the octahedral PC this fact is a decisive evidence that the investigated optical transitions indeed belong to the tetragonal PC whereby the Yb^{3+} ions are sitting on the octahedral site of the $KMgF_3$ host matrix.

The residual difference between the experimental and the calculated values of the g factors (Table III) can be explained by covalency effects which were neglected in the calculation of the CF parameters. The calculation of the g factors with the above functions gave different signs for $g_\parallel$ and $g_\perp$ (Table III). By taking this into account we obtained $\tilde{g}=-2.597$ [$g_{\rm cub}=-2.667$ for Γ_7 (Ref. 1)]. Thus the rule of the average g factor agrees with the model of an Yb^{3+} ion located in a basically octahedral position, contrary to the conclusion reached before.[3] As in the present situation the variant of a high crystal field applies, the rule of the average g factor is probably more general than initially formulated. Indeed, it does not depend on the relative magnitude between the cubic and the low-symmetry CF components acting on the RE ion. But it is necessary to take into account the true signs of the g factors, which are not always known. When only the absolute signs of the g factors are taken to evaluate $\tilde{g}$ then incorrect conclusions are obtained from this rule.[3]

The theoretical calculation of the THFI parameters A_i was carried out by including all the bonding mechanisms developed[21–25] for the RE ion-fluorine couples. We took into account not only the ground configuration but in addition excited ones of the RE ions. Knowledge of the true distances between the RE and the fluorine ions is of central importance in the aforementioned calculations. Note that the detailed structural deformation of the complex is unknown (save its tetragonal symmetry). This is true too for the distances between Yb^{3+} and F_{1-5}^-. They can be estimated, however, by comparing the obtained THFI parameters with results from the cubic PC with the aid of the following known relations. It is established that $\hat{B}=(h/\hat{g}\beta)\hat{A}$ is a true tensor, unlike $\hat{A}$ and that any nonsymmetric second-rank tensor can be decomposed into a symmetric and an antisymmetric part. By using appropriate transformations it is possible to obtain from the

TABLE III. Energy levels (cm^{-1}) and g factors of Yb^{3+} in $KMgF_3$.

J	Symmetry properties and g factors of energy levels	Experiment	Theory
$\frac{5}{2}$	$^4\Gamma_{t7}$	11 175	11 172
	$^3\Gamma_{t7}$	10 500	10 504
	$^3\Gamma_{t6}$	10 200	10 207
$\frac{7}{2}$	$^2\Gamma_{t6}$	1006	1013
	$^2\Gamma_{t7}$	700	704
	$^1\Gamma_{t7}$	105	106
	$^1\Gamma_{t6}$	0	0
	$g_\parallel(^1\Gamma_{t6})$	|1.070|	0.992
	$g_\perp(^1\Gamma_{t6})$	|4.430|	−4.496

TABLE IV. Crystal field (B_n^m) and spin-orbit interaction (ξ) parameters (in cm^{-1}) of Yb^{3+} in $KMgF_3$.

Symmetry	ξ	B_2^0	B_4^0	B_4^3	B_4^4	B_6^0	B_6^3	B_6^4	B_6^6	Ref.
Tetragonal	2904	850	39		1274	−1		137		this work
		40	−185	−6050		−10	−90		30	[a]
Trigonal		−63	−176	−5568		42	−246		389	[b]
	2903	−278	−221	−5450		−42	−220		490	[c]
Cubic			311			9				[a]
	2900		334			4				[c]

[a]Reference 7.
[b]Reference 6.
[c]Reference 19.

former part the isotropic (purely covalent) contribution to the THFI, called in the following B_s. Comparison of the B_s values obtained for $Yb^{3+}-F_{1-4}^-$ and $Yb^{3+}-F_5^-$, respectively, with the corresponding quantity from the cubic Yb^{3+} center (Table II) allowed us to identify the THFI parameter set which corresponds to the strong local deformation. Assuming that the Yb^{3+} substitutes for a host Mg^{2+} ion and is displaced towards the O^{2-} then an increase of the distance between the impurity ion and F_{1-4}^- is expected with a concomitant reduction of the covalency of these bonds. An additional reason for the increase of these distances is the large difference in ionic radius between Mg^{2+} and Yb^{3+} [$r_{Yb}^{3+}=0.87$ Å, $r_{Mg}^{2+}=0.63$ Å (Ref. 26)]. The appreciable gain of covalency observed for the bond to F_5^- can be explained by the important difference between the tetragonal Yb^{3+} ground-state wave function and the one of the cubic PC. Our results further prove that the tetragonal (for F_5^-) and the cubic THFI parameters are explained by the same set of covalency parameters. Therefore it is possible to conclude that the smallest distance between Yb^{3-} and F^- is determined by the sum of the two ionic radii [$r_F=1.33$ Å (Ref. 26)], i.e., $R(Yb^{3+}-F_{1-5}^-)\cong 2.2$ Å, to be compared with the distance between sites of 1.987 Å, in the undistorted lattice.

The overlap integrals were evaluated with Hartree-Fock wave functions of Yb^{3+}[27] and of fluorine.[28] The electron transfer energies, the radial $5s$, $5d$ functions and $5d$, $6s$, $6p$ functions, the $4f$-$5d$ and $4f$-$6s$ interaction parameters taken from Refs. 6, 29, and 30 were used. The mixing of the fluorine $1s$ and $2s$ shells was taken into account as well. The reduced matrix elements $W^{(1k)j}$ and $V^{(j)}$ for Yb^{3+} calculated by Falin *et al.*[6] were utilized. The following theoretical covalency parameter values produced best convergence with the experimental quantities: for F_5^-: $\gamma_{4fs}=0.025$, $\gamma_{4f\sigma}=-0.05$, $\gamma_{4f\pi}=0.05$, $\gamma_{5ds}=\gamma_{5d\sigma}=\gamma_{5d\pi}=0$; for F_i^- ($i=1...4$): $\gamma_{4fs}=0.01$, $\gamma_{4f\sigma}=-0.05$, $\gamma_{4f\pi}=0.05$, $\gamma_{5ds}=0.05$, $\gamma_{5d\sigma}=-0.3$, $\gamma_{5d\pi}=0.3$. The covalency parameters for the $6s$ and $6p$ shells were taken equal to γ_{5d}, whereas γ_{5p} was always set to zero. Previously determined[24] radial integrals were used. The $4f$-$5d$ interaction parameters G^1, G^3, and G^5 given by Starostin *et al.*[31] and the $4f$-$6s$ interaction parameter $G^3=2359\,cm^{-1}$ from Goldschmidt[32] were applied for Yb^{3+}.

In Table V are collected the numerical contributions obtained from the various mechanisms of the Yb^{3+} fluorine interaction which were included. These are: the dipole-dipole contribution including multipole corrections (H_{d-d}); the effect of overlap and covalency (H_{4f}); the processes of electron transfer into the empty $5d$ and $6s$ shell ($H_{5d,6s}$); the effects of mixing of the $4f$ and $5d$ states by the field of the virtual hole on the fluorine atom (H_{vh}) and by the odd crystal field ($H_{\text{odd field}}$); the sum of the effects of spin polarization of the $5s$ and $5p$ shells ($H_{5s\to 5d}, H_{5s\to 6s}, H_{5p\to 6p}$) $-(H_{\text{spin polar}})$. The sum of all these contributions and the experimental values of the corresponding THFI are given in the last two columns of this table. Note that the theoretical calculations only give good agreement with the experiment for the situation when the signs of $g_\parallel$ and $g_\perp$ are mutually different.

As shown in Table V, the theoretical model used for the determination of the THFI parameters A_i yields quite satis-

TABLE V. Theoretical values of the THFI parameters A_i (in MHz) for the first fluorine shell of Yb^{3+} in $KMgF_3$ (see text for details).

	$H_{d\text{-}d}$	H_{4f}	$H_{5d,6s}$	H_{vh}	$H_{\text{odd field}}$	$H_{\text{spin polar}}$	Total	Exper.
					F_5^-			
$A_1(A_\perp)$	16.3	3.1	0	0.3	2.5	1.5	23.7	23.30
$A_3(A_\parallel)$	7.6	53.2	0	5.4	−8.4	−1.2	56.6	57.63
					F_{1-4}^-			
A_1	−31.3	−3.8	11.9	−2.3	0	1.0	−24.5	−24.60
A_2	16.2	21.4	−26.0	16.2	0	−2.3	25.5	24.46
A_3	−3.3	0.9	2.4	1.4	0	0.8	2.2	2.18

factory agreement (the calculation for the parameters A_4 and A_5 was not carried out because of the smallness of these constants). The analysis of the separate non-dipolar contributions shows that for the tetragonal Yb^{3+} center in $KMgF_3$,[6] as well as for the cubic and the trigonal ones, polarization effects contribute very little to THFI. This is contrasting with other RE ion [for example, Gd^{3+},[23] Dy^{3+},[33] Er^{3+} (Ref. 23)].

ACKNOWLEDGMENTS

This work was supported by the Russian Foundation for Basic Research (Grant No. 99-02-17481) and by the Swiss National Science Foundation (Grant No. 7GUKA041276). The authors are grateful to G. M. Safiullin and I. I. Fazlizhanov for help with the experiment.

[1] K. R. Lea, M. J. M. Leask, and W. P. Wolf, J. Phys. Chem. Solids **23**, 1381 (1962).
[2] H. R. Lewis and E. S. Sabisky, Phys. Rev. **130**, 1370 (1963).
[3] M. M. Abraham, C. B. Finch, J. L. Kolopus, and J. T. Lewis, Phys. Rev. B **3**, 2855 (1971).
[4] M. L. Falin, V. P. Mejklyar, and V. A. Ulanov, Phys. Status Solidi B **84**, K29 (1977).
[5] M. L. Falin, V. P. Meiklyar, and A. L. Konkin, J. Phys. C **13**, 1299 (1980).
[6] M. L. Falin, M. V. Eremin, M. M. Zaripov, I. R. Ibragimov, and M. P. Rodionova, J. Phys.: Condens. Matter **2**, 4613 (1990).
[7] A. A. Antipin, A. V. Vinokurov, M. P. Davydova, S. L. Korableva, A. L. Stolov, and A. A. Fedii, Phys. Status Solidi B **81**, 287 (1977).
[8] M. L. Falin, I. I. Fazlizhanov, and M. M. Zaripov, *Extended Abstracts of the 27 Congress AMPERE, Magnetic Resonance and Related Phenomena* (Zavoisky Physical-Technical Institute, Kazan, Russia, 1994), Vol. 2, p. 426.
[9] V. F. Bespalov, M. L. Falin, B. N. Kazakov, A. M. Leushin, I. R. Ibragimov, and G. M. Safiullin, *Abstract Book of the International Conference on f-Elements* (Centre National de la Recherche Scientifique, Paris, France, 1997), p. 93.
[10] R. Lakowicz, *Principles of Fluorescence Spectroscopy* (Plenum Press, New York, 1983).
[11] W. DemtrÖder, *Laser Spectroscopy, Basic Concepts and Instrumentation* (Springer-Verlag, Berlin, 1982).
[12] B. N. Kazakov, A. V. Mikheev, G. M. Safiullin, and N. K. Solovarov, Opt. Spectrosk. **79**, 426 (1995) [Opt. Spectrosc. **79**, 392 (1995)].
[13] B. N. Kazakov, G. M. Safiullin, and N. K. Solovarov, R. U. Patent No. 2085021 (20 July 1997).
[14] V. F. Bespalov, M. L. Falin, B. N. Kazakov, A. M. Leushin, I. R. Ibragimov, and G. M. Safiullin, Appl. Magn. Reson. **11**, 125 (1996).
[15] M. M. Zaripov, I. R. Ibragimov, and M. L. Falin, Fiz. Tverd. Tela (Leningrad) **29**, 1546 (1987) [Sov. Phys. Solid State **29**, 887 (1987)].
[16] M. M. Zaripov, V. P. Meiklyar, and M. L. Falin, Pis'ma Zh. Eksp. Teor. Fiz **29**, 265 (1979) [JETP Lett. **29**, 237 (1979)].
[17] S. A. Altshuler and B. M. Kozyrev, *Electron Paramagnetic Resonance in Compound of Transition Elements* (Nauka, Moscow, 1972).
[18] V. F. Bespalov, B. N. Kazakov, A. M. Leushin, and G. M. Safiullin, Fiz. Tverd. Tela (St. Petersburg) **39**, 1030 (1997) [Phys. Solid State **39**, 925 (1997)].
[19] B. N. Kazakov, A. M. Leushin, G. M. Safiullin, and V. F. Bespalov, Fiz. Tverd. Tela (St. Petersburg) **40**, 2029 (1998) [Phys. Solid State **40**, 1836 (1998)].
[20] A. M. Leushin, *Tables of Functions Transforming According to the Irreducible Representations of Crystal Point Groups* (in Russian) (Nauka, Moscow, 1968).
[21] O. A. Anikeenok, M. V. Eremin, M. L. Falin, and V. P. Meiklyar, J. Phys. C **15**, 1557 (1982).
[22] O. A. Anikeenok, M. V. Eremin, M. L. Falin, A. L. Konkin, and V. P. Meiklyar, J. Phys. C **17**, 2813 (1984).
[23] O. A. Anikeenok, M. V. Eremin, and O. G. Khutsishvili, Fiz. Tverd. Tela (Leningrad) **28**, 1690 (1986) [Sov. Phys. Solid State **28**, 935 (1986)].
[24] M. L. Falin, M. V. Eremin, M. M. Zaripov, I. R. Ibragimov, A. M. Leushin, R. Yu. Abdulsabirov, and S. L. Korableva, J. Phys.: Condens. Matter **1**, 2331 (1989).
[25] M. L. Falin, M. V. Eremin, H. Bill, and D. Lovy, Appl. Magn. Reson. **9**, 329 (1995).
[26] R. D. Shanon and C. T. Prewitt, Acta Crystallogr., Sect. B: Struct. Crystallogr. Cryst. Chem. **25**, 925 (1969).
[27] *Physical Sciences Data 16, Gaussian Basis Sets for Molecular Calculations*, edited by S. Huzinaga (Elsevier Science Publishers, Amsterdam, 1984), p. 426
[28] E. Clementi and C. Roetti, At. Data Nucl. Data Tables **14**, 177 (1974).
[29] H. U. Van Piggelen, W. C. Nieuwpoort, and G. A. J. van der Velde, J. Chem. Phys. **72**, 3727 (1980).
[30] K. Rajnak, J. Chem. Phys. **37**, 2440 (1963).
[31] N. V. Starostin, P. F. Gruzdev, E. P. Pashinina, and V. A. Ganin, *Spektroskopija Kristallov* (Nauka, Moscow, 1975), p. 384.
[32] Z. B. Goldschmidt, *Handbook on the Physics and Chemistry of Rare-Earths* (North-Holland, Amsterdam, 1984), Chap. 1.
[33] M. L. Falin, V. A. Latypov, H. Bill, and D. Lovy, Appl. Magn. Reson. **14**, 427 (1998).